CELL CYCLE, 2018
VOL. 17, NO. 3, 377–389
https://doi.org/10.1080/15384101.2018.1426417

Taylor & Francis
Taylor & Francis Group

REPORT

Region specific knock-out reveals distinct roles of chromatin modifiers in adult neurogenic niches

Christopher T. Rhodes[a], Giulia Zunino[b], Shu-Wei Angela Huang[a], Sandra M. Cardona[a], Astrid E. Cardona[a,c], Mitchel S. Berger[d], Vance P. Lemmon[b] and Chin-Hsing Annie Lin[a,e]

[a]Department of Biology, University of Texas at San Antonio, San Antonio, TX 78249, USA; [b]The Miami Project to Cure Paralysis, University of Miami, Miami, FL 33136, USA; [c]South Texas Center for Emerging Infectious Diseases, University of Texas at San Antonio, TX 78249, USA; [d]Department of Neurological Surgery, University of California, San Francisco, CA, 94143, USA; [e]Neuroscience Institute, University of Texas at San Antonio, San Antonio, TX 78249, USA

ABSTRACT

Histone methyltransferases (HMTs) are present in heterogeneous cell populations within the adult brain including neurogenic niches. Yet the question remains whether loss of HMTs and the resulting changes in histone methylation alter cell fate in a region-specific manner. We utilized stereotaxic injection of Cre recombinant protein into the adult neurogenic niches, the subventricular zone (SVZ) adjacent to the lateral ventricle and the subgranular zone (SGZ) of the dentate gyrus. We confirmed that Cre protein was enzymatically active *in vivo* and recombination events were restricted to the vicinity of injection areas. In this study, we focus on using Cre mediated recombination in mice harboring floxed HMT: enhancer of zeste homolog 2 (EZH2) or suppressor of variegation homolog (Suv4-20h). Injectable Cre protein successfully knocked out either EZH2 or Suv4-20h, allowing assessment of long-term effects in a region-specific fashion. We performed meso-scale imaging and flow cytometry for phenotype analysis and unbiased quantification. We demonstrated that regional loss of EZH2 affects the differentiation paradigm of neural stem progenitor cells as well as the maintenance of stem cell population. We further demonstrated that regional loss of Suv4-20h influences the cell cycle but does not affect stem cell differentiation patterns. Therefore, Cre protein mediated knock-out a given HMT unravel their distinguishable and important roles in adult neurogenic niches. This Cre protein-based approach offers tightly-controlled knockouts in multiple cell types simultaneously for studying diverse regulatory mechanisms and is optimal for region-specific manipulation within complex, heterogeneous brain architectures.

ARTICLE HISTORY
Received 19 October 2017
Revised 21 December 2017
Accepted 7 January 2018

KEYWORDS
subgranular zone; subventricular zone; enhancer of zeste homolog 2 (EZH2); suppressor of variegation homolog (Suv4-20h)

Introduction

Methylation of lysines in histone tails is a critical post-translational modification that regulates diverse biological processes including cell cycle, development, differentiation, metabolism, and multipotency of stem cells. Conventional promoter-driven knock-out mouse models have demonstrated the importance of histone modifications in specific cell types in the adult brain. However, histone methylation occurs in all cells types and is vulnerable to regional changes in metabolism-associated methyl influx due to environmental effects or pharmaceutical inhibitors of methylation. Since metabolic effects or drugs generally do not function in a cell type-specific manner, we developed a method allowing knockout of genes of interest in multiple cell types using a penetrating peptide tagged Cre protein. We used this approach to examine the functional consequences of regional loss of histone methylation by performing regional knock-out of two independent methyltransferases in the adult neurogenic niches.

Multipotent neural stem progenitor cells (NSPCs) exist in two adult neurogenic niches, the subventricular zone (SVZ) adjacent to the lateral ventricle and the subgranular zone of the dentate gyrus (SGZ/DG). Neural stem cells (NSCs) give rise to progeny including neuroblasts, which undergo cell fate transition toward neuronal lineages [1–3]. The balance between NSC self-renewal and differentiation is maintained, in part, by epigenetic repression to prevent transcriptional noise of lineage-specific genes [4–9]. One such mechanism to inhibit transcription is post-translational modifications on histone tails, including trimethylation at histone 3 lysine 27 (H3K27me3) and trimethylation at histone 4 lysine 20 (H4K20me3). H4K20me3 is catalyzed by suppressor of variegation 4–20 homologs (Suv4-20h1/Suv4-20h2; human homologs KMT5B/KMT5C), collectively described as Suv4-20h. Our previous genomic study using endogenous NSPCs isolated from baboon brain identified putative targets of H4K20me3 that function in cell cycle, metabolism, and immune response [10]. Germline deletion of *Suv4-20h1/Suv4-20h2* by Mox2-Cre showed that Suv4-20h impaired the maintenance of lymphoid progenitors [11]. To date, there is no report assessing the long-term effect of loss of Suv4-20h in adult neurogenic niches. H3K27me3 is catalyzed by enhancer of zeste homolog 2 (EZH2) [12], which is ubiquitously expressed in a wide range of cell types including NSPCs

CONTACT Chin-Hsing Annie Lin Annie.lin@utsa.edu University of Texas at San Antonio, One UTSA Circle, BSB 2.03.24, San Antonio, TX78249.
Supplemental data for this article can be accessed at https://doi.org/10.1080/15384101.2018.1426417

residing in the SVZ and SGZ/DG of murine and non-human primate baboon brains [10]. Our previous study using a non-human primate baboon model suggests that H3K27me3 represses developmentally critical regulators involved in differentiation [10]. A study using a GFAP-Cre mediated conditional *Ezh2* knockout found that EZH2/H3K27me3 is critical for postnatal neurogenesis in the mouse SVZ [13]. Using Nestin-CreERT2 and tamoxifen inducible system to deplete *Ezh2* in the SGZ/DG showed that EZH2 is important for learning and memory capabilities in 6-week old mice [14]. However, considerable evidence has shown that tamoxifen administration is neurotoxic, resulting in impaired learning in rodents and impaired decision making in humans, even at dosages far below those used for recombination studies [15–18]. Such toxicity can affect long-term phenotypic analysis, requiring an alternative approach to overcome these confounding factors.

As EZH2/H3K27me3 and Suv4-20h/H4K20me3 are present in heterogeneous populations within adult neurogenic niches [10], we developed an alternative method to gain insight into the roles of EZH2/H3K27me3 or Suv4-20h/H4K20me3 in a wide range of adult NSPCs. Using conditional *Ezh2* and *Suv4-20h* mouse models, we delivered penetrating peptide tagged Cre protein into the adult SVZ and SGZ/DG via stereotaxic injection to assess the long-term *in vivo* effect of region-specific loss of EZH2/H3K27me3 or Suv4-20h/H4K20me3. Following injection, Cre protein crosses the plasma and nuclear membranes via an engineered transduction peptide (CTP) and a nuclear localization sequence (NLS), respectively. The Cre protein consists of bacteriophage P1 Cre recombinase, which specifically recognizes 34 base-pair loxP sequences flanking a DNA sequence corresponding to the enzymatic domain of *Ezh2* or *Suv4-20h*, resulting in their deletion. We demonstrated that Cre protein is readily and locally taken up by cells following stereotaxic injection into targeted brain regions to decrease EZH2 or Suv4-20h abundance. After region-specific reduction of EZH2 in the adult SVZ, we utilized the iDISCO protocol [19] for meso-scale imaging of mouse brains by light sheet fluorescent microscopy (LSFM) and found a drastic effect on doublecortin-positive (DCX^+) migrating neuroblasts. After Cre protein locally reduced EZH2 in the SGZ/DG, both immunohistochemistry (IHC) and flow cytometry demonstrated that loss of EZH2 affects the maintenance of NSPCs. To determine if this phenotype is specific in response to the abundance of EZH2, we stereotaxically injected Cre protein in the SGZ/DG of conditional *Suv4-20h* mice and utilized imaging flow cytometry to provide comprehensive quantification of recombination efficiency along with phenotype analysis. Imaging flow cytometry also allowed co-localization studies of cell markers while providing a means for unbiased cell counting that has not been reported in any study relevant to adult hippocampal neurogenesis. We found regional loss of Suv4-20h influences the cell cycle. Hence, Cre protein mediated knock-out of either *Ezh2* or *Suv4-20h* underscores the importance of distinguishing roles of EZH2/H3K27me3 from Suv4-20h/H4K20me3 in a region-specific manner. Taken together, we demonstrated a useful method for localized injection of cell-permeable Cre recombinase into mouse brain for the study of conditional knockouts in mosaic contexts. Importantly, this region-specific protein-based approach for genetic manipulation enables future *in vivo* studies to understand the role of diverse epigenetic regulators distributed in a range of cell types within complex tissue architectures.

Results

Recombinant Cre protein induces homologous recombination in vitro *and* in vivo

The development of cell-penetrating peptide (CPP) tagging-Cre fusion proteins has provided an alternative approach to introducing Cre into a cell, in addition to transgenic or viral transduction methods [20,21]. As a proof of principle, this Cre fusion protein containing a cell transduction peptide (CTP: APWHLSSQYSRT) and a nuclear localization sequence (NLS) has been successfully delivered to cardiac muscle via ultrasound guided injection [22]. To simplify the description of this NLS-Cre-CTP fusion protein, Cre protein is the denotation used throughout the text.

To evaluate the long-term utility of Cre protein induced recombination *in vivo*, we delivered Cre protein via stereotaxic injections into the brains of adult R26R-lacZ or R26R-EYFP (denoted by *ROSA26*) (Supplementary Fig. 1A-1E). Injection coordinates were empirically derived using fluorescent red retrobeads (Supplementary Fig. 1F-1H). Within the SVZ of R26R-lacZ mice injected with Cre protein, constitutive β-galactosidase (β-gal) expression was restricted to injection sites indicating that Cre protein injection induces recombination within targeted sites in a highly localized manner (Supplementary Fig. 2). Injection sites were largely demarcated from surrounding areas, as only minor β-gal expression was observed in cells outside the injection site. Using image flow cytometry analysis, we confirmed the high efficiency of Cre-mediated recombination within the injected areas of R26R-EYFP mice (Supplementary Fig. 3). Immediately following dissection of hippocampal tissue for flow cytometry, cells from Cre protein injected hemispheres displayed YFP expression in regions corresponding to injection sites (Supplementary Fig. 3B, 3C). Cells from Cre injected hemispheres increased 519% in YFP^+ populations compared to hemispheres injected with vehicle solution (20% glycerol in PBS) (Supplementary Fig. 3D-3G). The ability of injected Cre protein to induce recombination localized to injection sites presents a novel approach in which genes can be genetically manipulated *in vivo* in a spatially-restricted manner. Importantly, our method leads to applications involving conditional knockout of small populations of cells and also genes expressed across multiple cell types simultaneously, such as examining the long-term regional effect of chromatin modifiers within neurogenic niches.

Conditional loss of EZH2 or Suv4-20h function in adult SVZ and SGZ/DG by recombinant Cre protein

The chromatin modification enzymes EZH2 and Suv4-20h, as well as resulting histone modifications, H3K27me3 and H4K20me3, respectively, are ubiquitously present in a wide range of cell types in the adult SVZ and SGZ/DG. Within these neurogenic niches, such cell types include NSCs expressing GFAP and/or Nestin, and DCX^+ neuroblasts (NBs)

(Supplementary Fig. 4–6). The SGZ/DG also contains differentiated cell types including βIII-Tubulin$^+$ immature neurons and NeuN$^+$ mature neurons (Supplementary Fig. 5–6). To delineate which subpopulations are most impacted by the loss of EZH2 or Suv4-20h, we utilized stereotaxic injection of Cre protein into targeted sites within the adult SVZ and SGZ/DG of conditional *Ezh2* or *Suv4-20h1* mouse models. These mouse models harbor floxed alleles of genomic sequence encoding the enzymatic SET domain of *Ezh2* (*Ezh2*$^{flox/flox}$)[12] or *Suv4-20h1* (*Suv4-20h1*$^{flox/flox}$;*Suv4-20h2*$^{-/-}$) [11]. To monitor knock-out efficiency, we bred *Ezh2*$^{flox/flox}$ mice or *Suv4-20h1*$^{flox/flox}$;*Suv4-20h2*$^{-/-}$ mice to R26R-lacZ or R26R-EYFP mice (denoted by *ROSA26*) with loxP sites flanking a stop cassette upstream of β-galactosidase (β-gal) or yellow fluorescent protein (YFP). The crosses resulted in homozygous alleles denoted by *Ezh2*$^{flox/flox}$;*ROSA26* and *Suv4-20h1*$^{flox/flox}$;*Suv4-20h2*$^{-/-}$;*ROSA26* mouse colonies for experiments. Following stereotaxic injection, the Cre protein was capable of crossing the plasma membrane of adjacent cells, importing into the nucleus, and initiating recombination at loxP flanked target sites. Such Cre mediated recombination resulted in excision of the SET domain of EZH2 (or Suv4-20h) as well as the stop cassette upstream of the *ROSA26* reporter to achieve simultaneous ablation of EZH2 (or Suv4-20h) catalytic activity and constitutive expression of β-gal (or YFP) (Supplementary Fig. 2–3). In parallel with phenotypic analysis, RT-qPCR confirmed a significant 2.63 (range from 1.7 to 4.4) fold knock-down of *Ezh2* mRNA in Cre injected hemispheres compared to controls (Supplementary Fig. 7A) in *Ezh2*$^{flox/flox}$;*ROSA26* mice, 19 days post Cre injection into SGZ/DG. Sustained knock-down of *Ezh2* mRNA was detectable within 3.66-fold reduction at 32 days post Cre injection (data not shown). In addition, we validated the expression levels of EZH2/H3K27me3 putative targets identified from our previous study using RT-qPCR [10]. We demonstrated that *Pax5* increased ($p < 0.003$) following knock-down of *Ezh2* transcript while *Hmx1, Hoxa5, Hoxc6, Hoxd13, Mnx1, Osr2, and Sp9* decreased ($p < 0.05$) 19 days post Cre injection into SGZ/DG (Supplementary Fig. 7A-C). Moreover, Cre mediated recombination was highly efficient as virtually all β-gal-positive cells lacked H3K27me3 within injection sites of the SVZ (Supplementary Fig. 7D-G).

EZH2/H3K27me3 influences differentiation paradigm and maintenance of NSPCs in the mouse SVZ and SGZ/DG

To explore how differential H3K27me3 enrichment due to diminished EZH2 activity affected the cell fate of NSPCs in the SVZ, we assessed the change in NSPC subpopulations at 10 and 32 days post-Cre protein injection into the SVZ of *Ezh2*$^{flox/flox}$;*ROSA26* (experimental group) and *ROSA26* reporter mice (control group). Ten days corresponded to the times required for SVZ NSCs to be repopulated while 32 days corresponded to the time period for SVZ NSPC differentiation [1,2]. Ten days post-Cre protein injection within the SVZ resulted in a significant decrease in the proportion of H3K27me3-positive cells of *Ezh2*$^{flox/flox}$;*ROSA26* mice compared to controls (p-value = 0.007) (Figure 1(B)). Additionally, there was a substantial increase of H3K27me3$^-$/DCX$^+$ migrating NBs within the SVZ compared to control mice (Figure 1(C–S)). This phenotype was observed in the SVZ of multiple animals 10 days after Cre injection. Further, 32 days after Cre protein injection, immunostaining was used to assess NSPC populations within the SVZ including GFAP, Nestin, and DCX. Thirty-two days after injection, Cre injected SVZ of *Ezh2*$^{flox/flox}$;*ROSA26* mice resulted in a significant decrease in H3K27me3-positive cells within the dorsal SVZ compared to controls (p-value = 0.002) (Figure 2(A)) while there was an increase in the H3K27me3$^-$/DCX$^+$ population 32 days after Cre injection into *Ezh2*$^{flox/flox}$;*ROSA26* mice compared to controls (Figure 2(B–J), Supplementary Fig. 8). However, 32 days post Cre injection into *Ezh2*$^{flox/flox}$;*ROSA26* mice did not show a significant change in either GFAP$^+$ or Nestin$^+$ populations compared to controls (Cre injected into *ROSA26* mice). Immunohistochemistry (IHC) results from 10 day post-Cre protein injected SVZ showed a decrease in DCX$^+$ NBs along the RMS, suggesting NBs migrate away from the SVZ earlier than 10 days. In this regard, a shorter time point of 5 days post-Cre protein injection was chosen to detect early NBs migration, using sagittal sections (Supplementary Fig. 9). Compared to vehicle injected controls, Cre injected hemispheres showed a moderate decrease in DCX$^+$ NBs at the dorsal SVZ and substantial increases in DCX$^+$ NBs along the RMS and migrating tangentially into the olfactory bulb (OB) (n = 4). To further assess the migratory capacity of NBs along the RMS to the OB by meso-scale imaging, we utilized a modified iDISCO tissue clearing protocol and LSFM to examine DCX$^+$ populations originating from the SVZ. Consistent with our short- and long-term IHC data, iDISCO showed DCX$^+$ populations substantially increased in the dorsal SVZ and along the RMS upon Cre-mediated loss of EZH2/H3K27me3 after 5 days (Figure 3(B–D), Supplementary Fig. 10A-10E) while a moderate increase in DCX$^+$ cells was still detected in animals injected with Cre compared to vehicle (Figure 3(E–G), Supplementary Fig. 10F-10G) after 32 days post-injection. In addition, βIII-Tubulin$^+$ and NeuN$^+$ populations increased in the OB 10 days after loss of EZH2/H3K27me3 (Supplementary Fig. 11), as did the interneuron marker Calbindin (Supplementary Fig. 12).

The ubiquitous abundance and distribution of H3K27me3 among NSPCs within the SGZ/DG (Supplementary Figure 5) suggested distinct regulation by H3K27me3 in this adult neurogenic niche and compelled further investigation. We assessed the effect of loss of EZH2/H3K27me3 at 19, 32, or 46 days after stereotaxic injection of Cre into the SGZ/DG, which corresponded to the times required for NSPC proliferation, differentiation/migration, and integration into neuronal circuit, respectively [2,3]. In the SGZ/DG, we observed a notable increase in NeuN$^+$ (Figure 4(A,B)) and a moderate increase in Nestin$^+$ cells but no change in GFAP$^+$ cells at 19 days post-Cre injection compared to vehicle injected controls (Supplementary Fig. 13). Although the populations of DCX or βIII-Tubulin populations were not substantially changed 19 days after Cre injection (Supplementary Fig. 14), unusual colocalization of DCX$^+$/NeuN$^+$ cells was more abundant in the Cre injected SGZ/DG compared to vehicle injected SGZ/DG 19 days after injections (Figure 4(C–G)). Consistent with the 19 days immunohistochemistry data, flow cytometry analysis of SGZ/DG 32 days after Cre injection demonstrated an increase in NeuN$^+$ neurons (Figure 5). Intriguingly, 46 days after Cre injection

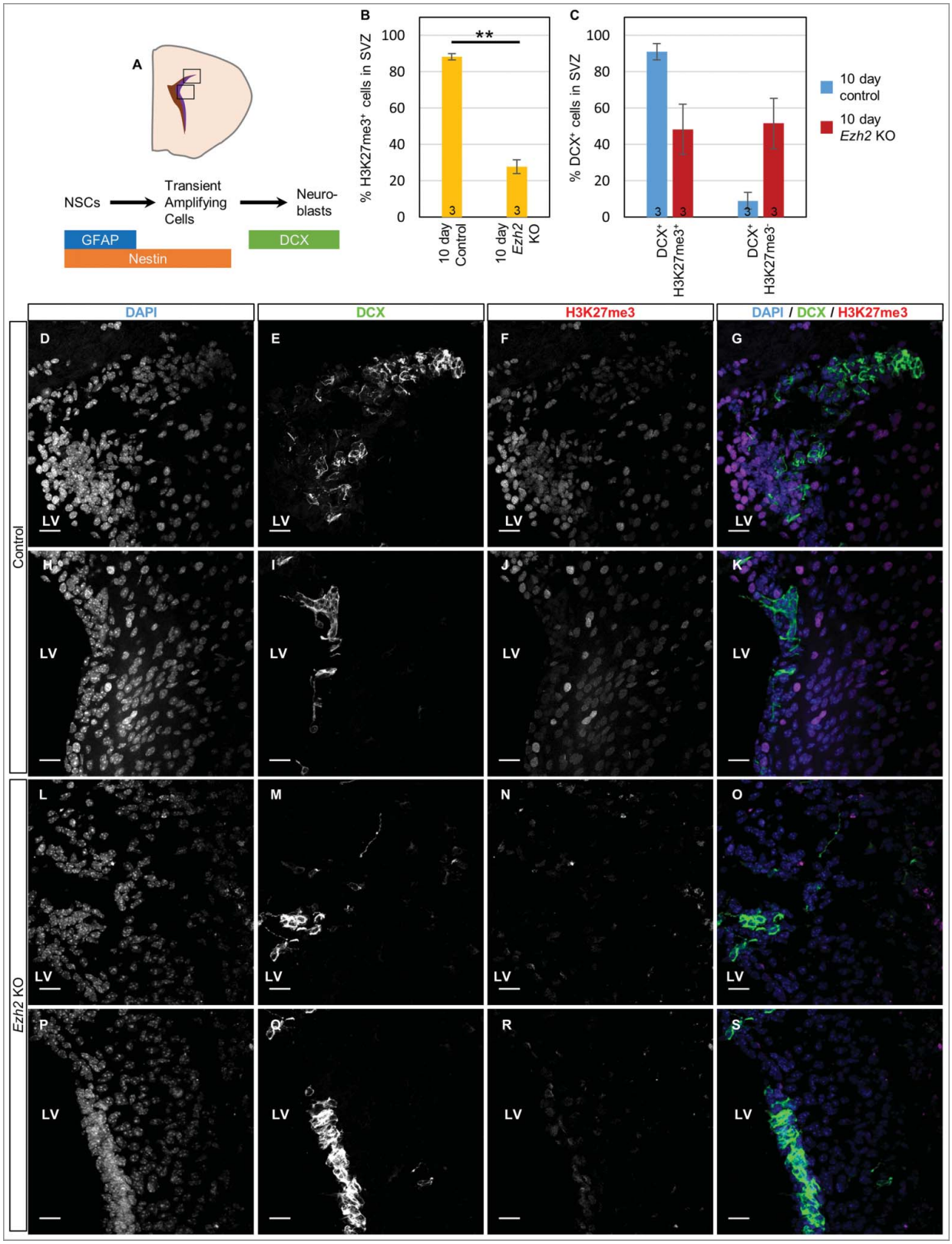

Figure 1. Loss of EZH2 affects neuroblasts within the subventricular zone. (A) Schema of coronal sectioned mouse brain containing subventricular zone (SVZ). Black boxes indicate regions imaged. Horizontal bars depict stepwise cell fate transition of NSPC. (B) Bar graph of the percentage of H3K27me3-positive cells present in the dorsal SVZ of *ROSA26* or *Ezh2*$^{flox/flox}$;*ROSA26* mice, 10 days post-injection of Cre. n = 3 mice per experimental group is indicated at base of bar graph, p-value = 0.007, determined using a Welch two sample t-test. (C) Percentage of DCX^{+}H3K27me3^{+} and DCX^{+}H3K27me3^{-} cells within the dorsal SVZ of *ROSA26* or *Ezh2*$^{flox/flox}$;*ROSA26* mice, 10 days post-injection of Cre. n = 3 mice per experimental group, standard error of the mean displayed on bars. (D-K) Immunostaining for doublecortin (DCX) and H3K27me3 in coronal sections obtained from the SVZ of a *ROSA26* mouse, 10 days post-injection of Cre, 40X. (L-S) Immunostaining for doublecortin (DCX) and H3K27me3 in the SVZ of an *Ezh2*$^{flox/flox}$;*ROSA26* mouse, 10 days post-injection of Cre, 40X. Scale bars = 20 μm.

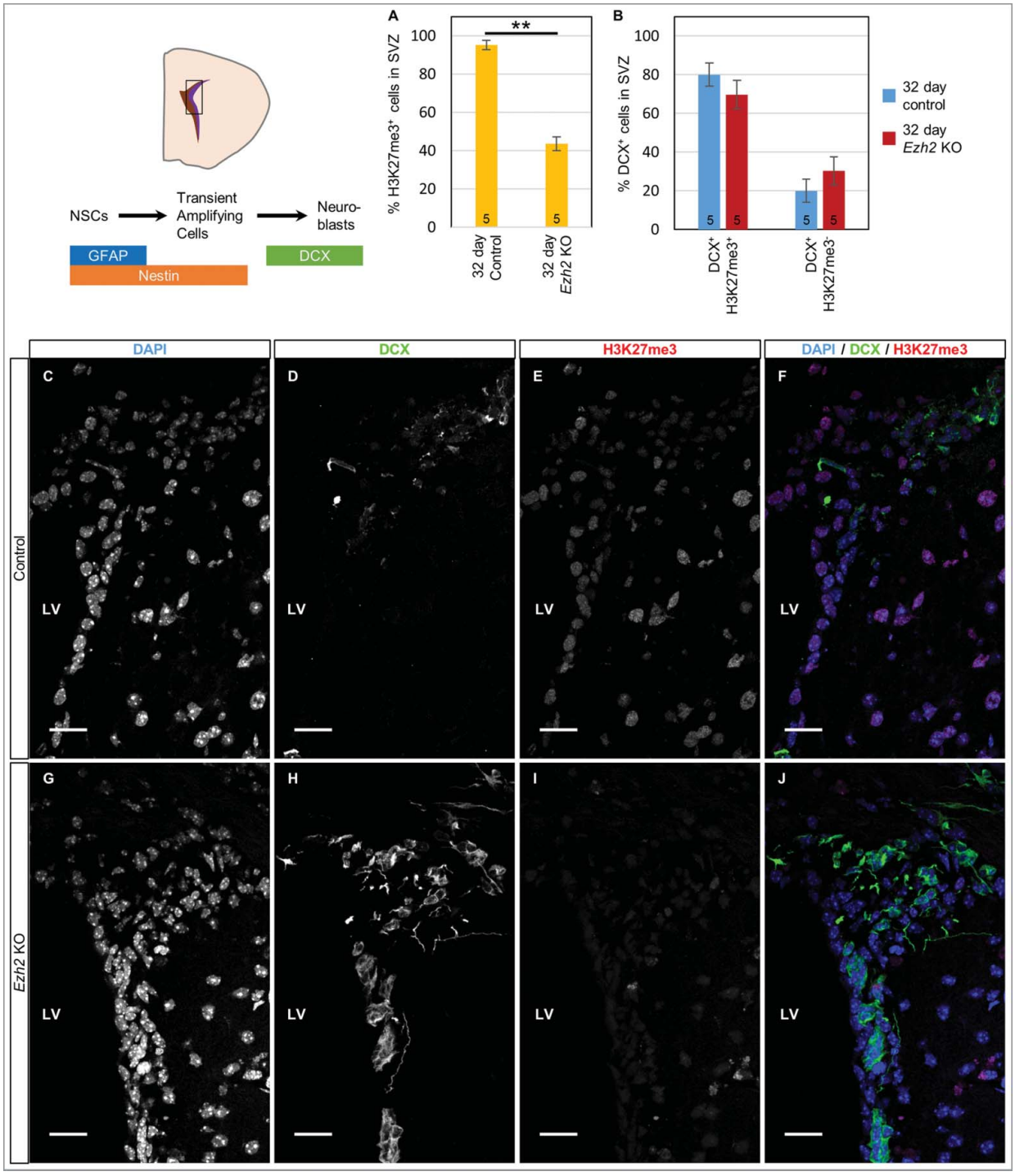

Figure 2. Sustained loss of EZH2 affects neuroblasts within the subventricular zone. (A) Bar graph of the percentage of H3K27me3-positive cells present in the dorsal SVZ of *ROSA26* or *Ezh2*$^{flox/flox}$;*ROSA26* mice, 32 days post-injection of Cre. n = 5 mice per experimental group is indicated at base of bar graph, p-value = 0.002, determined using a Welch two sample t-test. (C) Percentage of DCX^{+}H3K27me3^{+} and DCX^{+}H3K27me3^{-} cells within the dorsal SVZ and RMS of *ROSA26* or *Ezh2*$^{flox/flox}$;*ROSA26* mice, 32 days post-injection of Cre. n = 5 mice per experimental group, standard error of the mean displayed on bars. (C-F) Immunostaining for doublecortin (DCX) and H3K27me3 in coronal sections obtained from the SVZ of a *ROSA26* mouse, 32 days post-injection of Cre, 40X. (G-J) Immunostaining for doublecortin (DCX) and H3K27me3 in the SVZ of an *Ezh2*$^{flox/flox}$;*ROSA26* mouse, 32 days post-injection of Cre, 40X. Scale bars = 20 μm.

into SGZ/DG, Nestin^{+} populations were substantially increased, while a moderate decrease in NeuN^{+} neurons was detected compared to vehicle injected SGZ/DG (Supplementary Fig. 15). Findings from three time-point analyses suggest that regional loss of EZH2/H3K27me3 in the adult SGZ/DG induced early differentiation at 19- and 32-day while Nestin^{+} cells replenished NSPCs in response to declined NeuN^{+} population at extended 46-day. Collectively, our results showed distinguishable cellular phenotypes, in which the DCX^{+} population in the SVZ and the NeuN^{+} population in the SGZ/DG were the most affected upon regional loss of EZH2/H3K27me3.

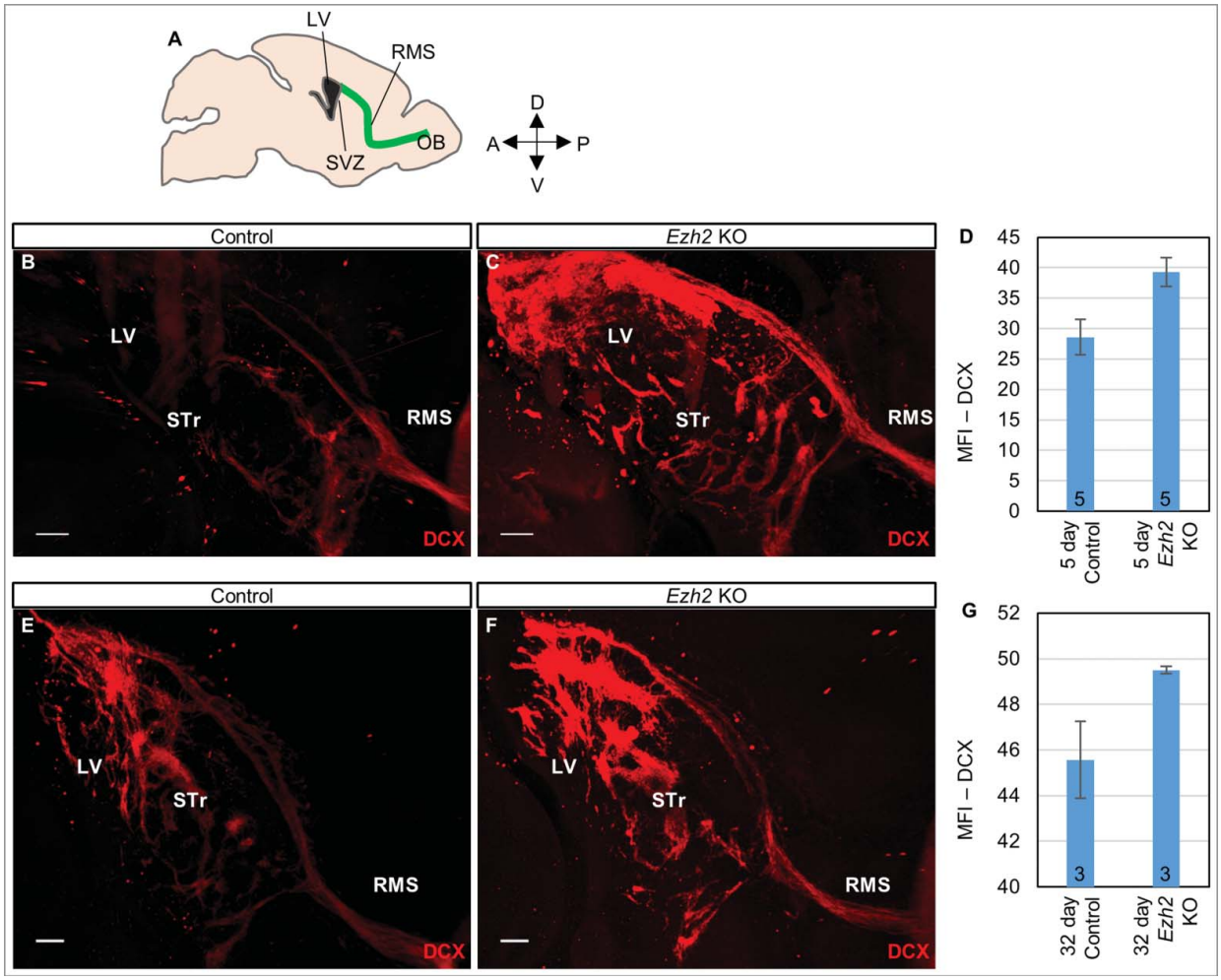

Figure 3. Loss of EZH2 alters neuroblast migration. (A) Scheme depicting sagittal sectioned adult mouse brain containing SVZ, RMS and OB. (B-G) Brain was sectioned along sagittal plane to a thickness of 2 mm prior to iDISCO based DCX detection (i.e. anti-DCX antibody incubation and tissue clearing). (B) Light sheet imaging of *Ezh2*$^{flox/flox}$;*ROSA26* forebrain, 5 days post-injection of vehicle. (C) Light sheet imaging of forebrain from *Ezh2*$^{flox/flox}$;*ROSA26* mouse 5 days post-injection (DPI) of Cre indicates increased DCX^{+} cells along dorsal SVZ, RMS, and nearby striatum. (D) Pixel mean fluorescence intensity (MFI) within automatically determined threshold regions containing DCX signal. (E) Light sheet imaging of forebrain of *Ezh2*$^{flox/flox}$;*ROSA26* mouse, 32 days post-injection of vehicle. (F) Light sheet imaging of forebrain of *Ezh2*$^{flox/flox}$;*ROSA26*, 32 days post-injection of Cre, with pixel MFI in threshold regions shown in (F). Scale bars = 200 μm. Numbers at base of bars in graph indicate sample size per experimental group for Welch two sample t-test.

Suv4-20h/H4K20me3 affects cell cycle of the adult NSPCs

Our previous study implicated Suv4-20h/H4K20me3 in regulating the cell cycle of NSPCs in the SVZ and inspired assessment of potential regulatory roles in the SGZ/DG [10]. Using the Cre protein approach, we assessed changes in NSPC populations and proliferation in *Suv4-20h1*$^{flox/flox}$;*Suv4-20h2*$^{-/-}$;*ROSA26* mice following Cre protein (experimental) or vehicle (control) injection into the SGZ/DG at the time points of 19, 32, and 46 days post injection. Two hours EdU labeling is commonly utilized for embryonic and postnatal neurogenesis studies. However, 19, 32, and 46 days post-Cre injection resulted in no significant change in numbers of 5-ethynyl-2'-deoxyuridine (EdU) labeled cells for 2 hours post-EdU injections (Supplementary Fig. 16–18). As adult neurogenesis is a slow process, our validation of proliferation rate in the SGZ/DG of adult mice indicated that a 12-hour EdU labeling was deemed suitable for examining NSPC proliferation (Supplementary Fig. 19). Intriguingly, 46 days post-Cre injection resulted in marginally increased numbers of EdU labeled cells 12 hours after EdU injection (Figure 6). However, no significant change in mitosis markers (i.e. phospho-H3(S10) or phospho-S780-Rb) and cell type markers (i.e. GFAP^{+}, DCX^{+}, or NeuN^{+} cells) was observed in subpopulations of NSPCs within the SGZ/DG 19, 32, or 46 days after Cre or vehicle injection (Figure 6(H–K), Supplementary Fig. 16–18, 20). Taken together, proliferation was consistently affected upon loss of Suv4-20h/H4K20me3 in the SGZ/DG and substantiate our previous findings that loss of Suv4-20h/H4K20me3 alters the S-phase of the cell cycle in the SVZ [10]. Our results suggest an essential role for Suv4-20h/H4K20me3 in cell cycle regulation during adult neurogenesis. Further, the Cre protein based approach allowed us to monitor potential long-term phenotypes following reduction of Suv4-20h. Intriguingly, long-term knockout of Suv4-20h/H4K20me3 in the adult neurogenic niche resulted in instances of seizures over the one year post-treatment period (Data not shown).

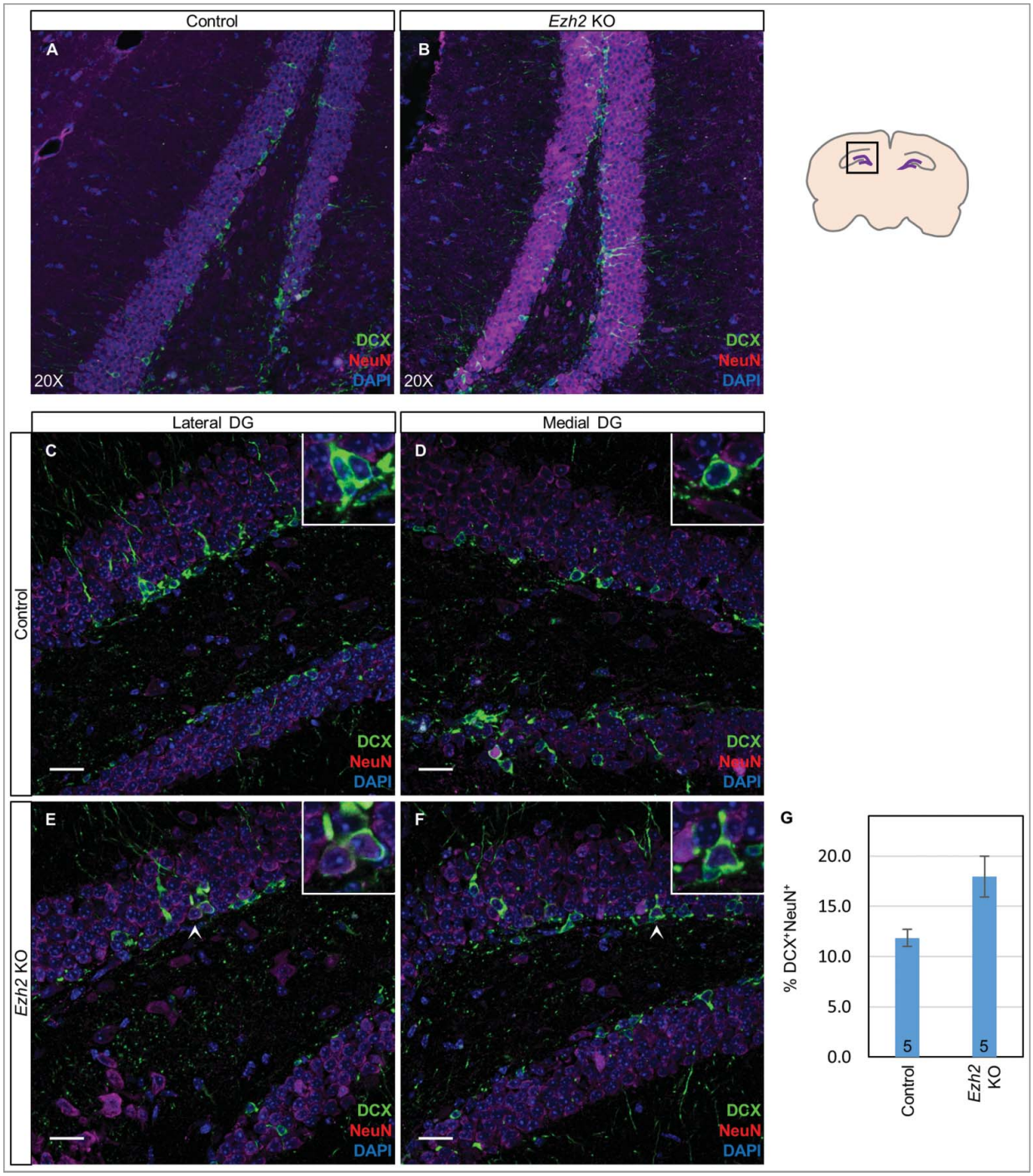

Figure 4. Loss of EZH2 alters cell fate transition in the subgranular zone of the dentate gyrus (SGZ/DG). (A-B) SGZ/DG was immunostained to detect DCX^+ neuroblasts and $NeuN^+$ mature neurons of *Ezh2*$^{flox/flox}$;*ROSA26* mouse 19 days post-injection of vehicle (A) or 19 days post-injection of Cre (B), 20X. Representative images of the lateral DG (C and E) and medial DG (D and F) of *Ezh2*$^{flox/flox}$;*ROSA26* mouse, 19 days post-injection of vehicle (C and D) or 19 days post-injection of Cre (E and F). Arrows in (E, F) indicate $DCX^+/NeuN^+$ cells. (G) Bar graph of the percentage of $DCX^+/NeuN^+$ cells present in the DG of *Ezh2*$^{flox/flox}$;*ROSA26* mice, 32 days post-injection of vehicle or Cre as quantified by flow cytometry. n = 5 mice per experimental group is indicated at base of bar graph. Scale bars = 20 μm. Insets = 40X.

Discussion

A challenging and yet unresolved obstacle in genetic manipulations of mice is altering gene expression in tissue composed of heterogeneous cell types. Such heterogeneity is common in virtually all adult stem cell niches, such as bone marrow, germ cell niches, and neurogenic niches. In such environments, there are circumstances where it would be beneficial to globally knockout a gene of interest across all cell types and examine any resulting phenotypes. For cell-type specific studies, a well-defined promoter can be applied to target a cell type of interest. For region-specific studies, our method of stereotaxic delivery of recombinant Cre protein presents a novel approach for a temporally and spatially-restricted knockout of a gene of interest. Injectable Cre proteins will not supplant other methods of tissue specific gene manipulation, including transgenic promoter-

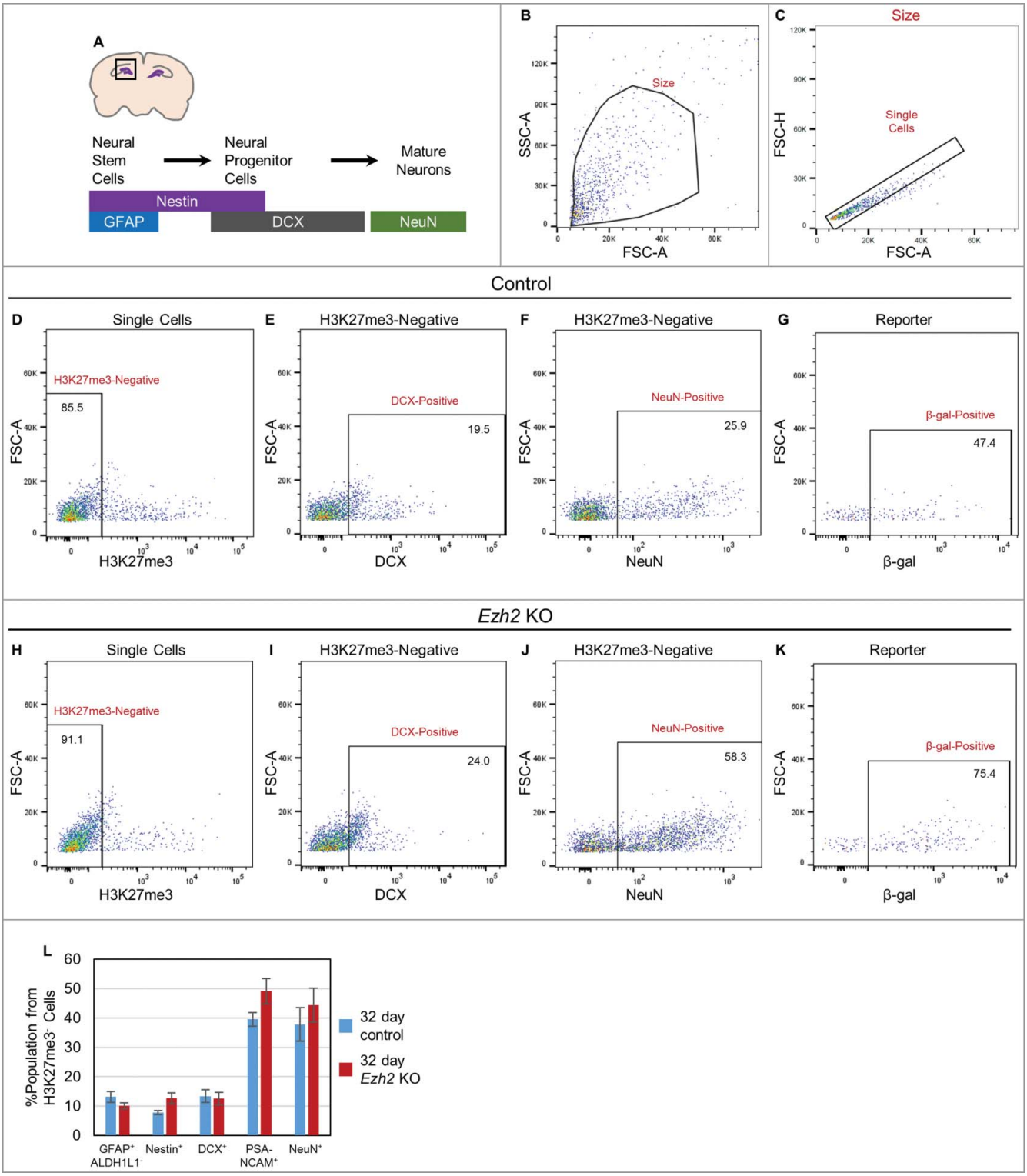

Figure 5. NSPC populations are altered following 32 day loss of EZH2 in the SGZ/DG. (A) Schematic of NSPC markers in the SGZ/DG. Horizontal bars depict markers expressed during stepwise cell fate transition of NSPCs in the SGZ/DG. (B-K) Representative flow cytometry analysis of isolated cells from SGZ/DG shows gating strategy based on SSC-A/FSC-A (B), single cells (C), and H3K27me3-negative population in *Ezh2*$^{flox/flox}$;*ROSA26* mouse, 32 days post-injection of vehicle (control) (D-G) or Cre (*Ezh2* KO) (h-k). (E-G) Vehicle injected hemisphere. Lineage specific H3K27me3^{-}DCX^{+} (E), H3K27me3^{-}NeuN^{+} (F), and H3K27me3$^{-}\beta$-gal^{+} populations (G). (I-K) Cre injected hemisphere. Lineage specific H3K27me3^{-}DCX^{+} (I), H3K27me3^{-}NeuN^{+} (J), and H3K27me3$^{-}\beta$-gal^{+} populations (K). (L) Bar graph presents abundance of lineage specific populations. n = 5 mice per experimental group, differences between conditions tested using a Welch two sample t-test.

driven expression, viral expression systems, or tamoxifen/tetracycline inducible systems. However, our Cre protein approach is useful for gene manipulation within selected injection sites that results in Cre-induced recombination in targeted regions without exogenous Cre expression; the Cre gene was neither integrated into the host genome, nor maintained extra-chromosomally on a non-integrating vector. The high spatial precision of our technique for manipulating target cells offers

A

Population	46 day control		46 day *Suv4-20h1* KO		p-value
	% Parent Gated - mean	% Parent Gated - SD	% Parent Gated - mean	% Parent Gated - SD	
All	100	0	100	0	NA
Focus	95.68666667	2.387055369	96.67	2.057304061	NA
Singlets	65.35666667	7.767170227	67.42333333	9.539393761	NA
Cells	56.2	4.655523601	58.68666667	3.765001107	NA
EdU	80.13333333	3.319824293	86.40666667	2.378578007	0.06247

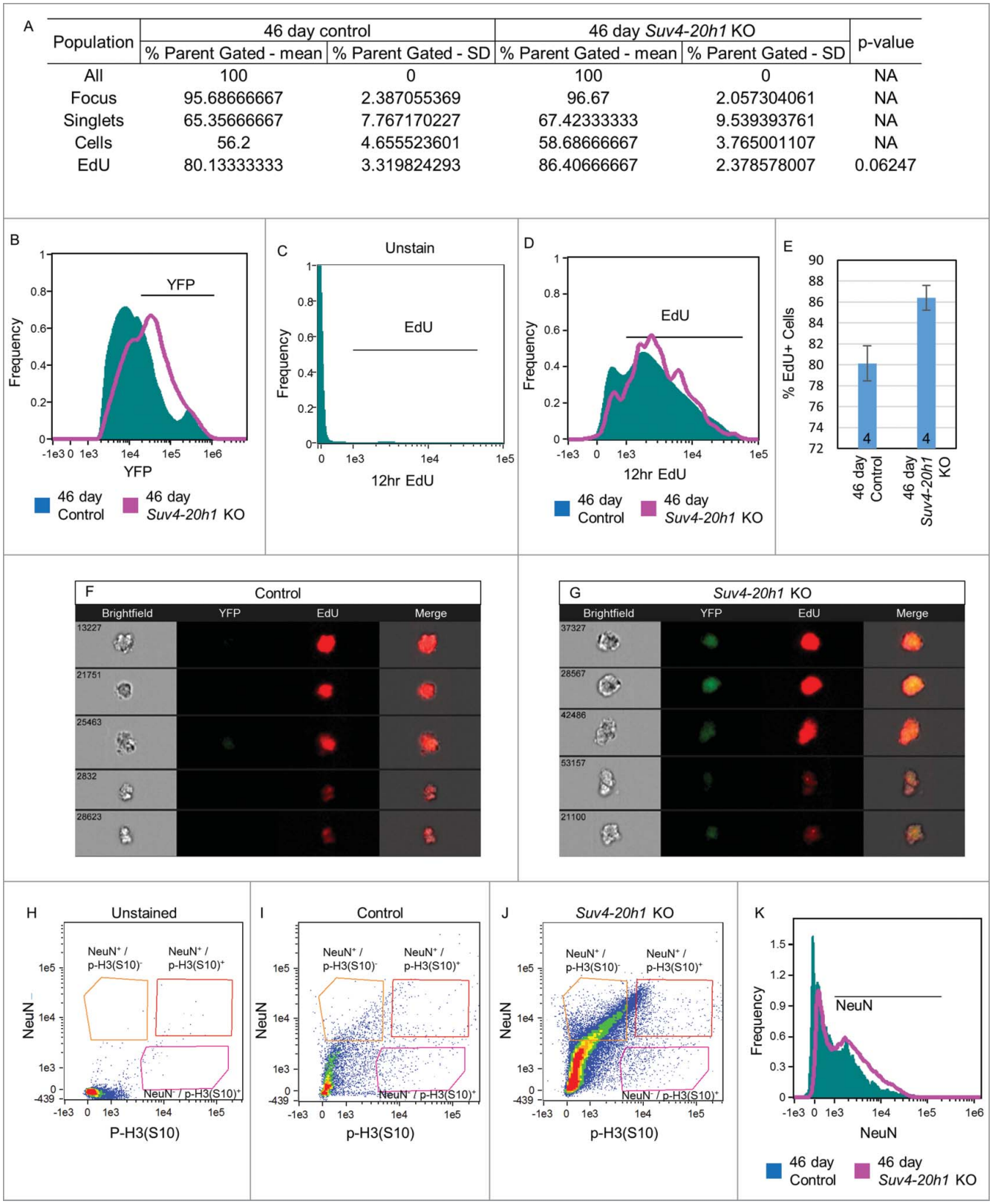

Figure 6. Suv4-20h mediates S-phase progression of NSPCs within the adult hippocampus. (A) Table indicating gating scheme used for population analyses, including test populations, mean % of parent population, standard deviation of each population and p-value, if applicable, for control and *Suv4-20h1* knockout experimental groups. (B) Histogram of YFP expression in SGZ/DG cells from vehicle or Cre injected hemispheres of *Suv4-20h*$^{flox/flox}$;*ROSA26*$^{Y/Y}$ mouse, 46 days post-injection. (C-D) Histogram of EdU in SGZ/DG cells from unstained population (C), and vehicle or Cre (D) injected hemispheres of *Suv4-20h*$^{flox/flox}$;*ROSA26*$^{Y/Y}$ mouse, 46 days post-injection. (E) Bar graph of the percentage of 12 hr. EdU-positive cells present in the DG of *Suv4-20h*$^{flox/flox}$;*ROSA26*$^{Y/Y}$ mice, 46 days post-injection of vehicle or Cre. n = 4 mice per experimental group, standard error of the mean displayed on bars. (F-G) Representative images of 12 hr. EdU labeled cells from vehicle injected (F) or Cre injected (G) hemispheres of *Suv4-20h*$^{flox/flox}$;*ROSA26*$^{Y/Y}$ mouse, displaying brightfield, YFP, EdU and merged channels. (H-J) NeuN and phospho-H3(S10) in SGZ/DG cells from unstained population (H), vehicle injected (I), and Cre injected (J) hemispheres of *Suv4-20h*$^{flox/flox}$;*ROSA26*$^{Y/Y}$ mouse, 46 days post-injection. (K) Histogram of NeuN^{+} neurons from vehicle and Cre injected hemispheres of *Suv4-20h*$^{flox/flox}$;*ROSA26*$^{Y/Y}$ mouse, 46 days post-injection.

enhanced modeling capabilities in murine models that would be useful for lineage tracing and cell fate studies at extended time-points. Future applications of such a system include region-specific gene knockout followed by single cell transcriptomic or microfluidic drug treatment to glean valuable insight into regulatory mechanisms at the molecular level within a heterogeneous population.

The combination of conditional HMT deletion and *ROSA26* reporter expression co-localized to a given injection site has utility in dissecting the role of various HMTs in complex processes such as cell fate transition. Within injection sites of the SVZ or SGZ/DG, two distinct populations of cells were observed following Cre recombination: cells with elevated levels of β-galactosidase and decreased histone modifications (i.e. cells having undergone Cre recombination), and cells with endogenous β-galactosidase levels, but high enrichment of histone methylation (i.e. cells which have not undertaken Cre recombination). The co-occupancy of both populations within an injected region acts as an internal control, and becomes useful in probing the role of HMTs in cell autonomous or non-cell autonomous regulations within these neurogenic niches. Utilizing this novel region-specific gene manipulation in parallel with modified iDISCO whole brain imaging and quantitative image flow cytometry, we have demonstrated that EZH2/H3K27me3 plays an important role in the maintenance of subpopulations within the SVZ and the SGZ/DG. Thus, our finding adds to a compendium of previous studies on the role of EZH2 in NSPCs using promoter-specific conditional knockout methods [5,6,13,14]. In addition, while cancer treatment using EZH2 inhibitors to target dysregulation of EZH2/H3K27me3 in glioblastoma subtypes is ongoing, our Cre protein-based manipulation uncovers long-term *in vivo* effects upon loss of EZH2. The concept of non-cell type specific manipulation described in this work can be applied to modeling long-term *in vivo* effect of other epigenetic modifiers prior to the development and investment of drug inhibitors for therapeutics. Moreover, our study is the first demonstration that the cell cycle within adult neurogenic niches is regulated, at least in part, by Suv4-20h/H4K20me3.

Our approach is not limited to neurogenic niches, and can be successfully implemented in various models to address myriad tightly-controlled knockouts or knock-ons in many tissues or cells simultaneously. As a broader impact, our novel approach for gene manipulation is optimal for studying many other regulatory mechanisms in a site-specific fashion, and can be applied to additional brain regions and/or to targeted cell populations within complex, heterogeneous tissue architectures. In addition, this method would be particularly useful for investigating developmentally critical genes in localized regions of solid organs, where complete deletion *in utero* would result in embryonic or perinatal lethality. Furthermore, use of recombinant proteins for *in vivo* transduction of therapeutic protein has already been performed to protect against cerebral infarction, ischemic brain injury, and neural apoptosis, via intraperitoneal injection in mice [23,24]. Therefore, the cell permeable proteins like CTP-tagged protein used in this study could be potentially adapted for production of recombinant pharmaceutical proteins for therapeutic applications.

Methods

Animal models

Mice contained a floxed SET domain of EZH2 (*Ezh2*$^{flox/flox}$) or Suv4-20h (*Suv4-20h1*$^{flox/flox}$;*Suv4-20h2*$^{-/-}$). *Ezh2*$^{flox/flox}$ mice or *Suv4-20h1*$^{flox/flox}$;*Suv4-20h2*$^{-/-}$ mice were crossed to R26R-lacZ or R26R-EYFP reporter mice (Jackson laboratory) (denoted by *ROSA26*) with loxP sites flanking a stop cassette upstream of β-galactosidase (β-gal) or yellow fluorescent protein (YFP). The crosses resulted in *Ezh2*$^{flox/flox}$;*ROSA26* and *Suv4-20h1*$^{flox/flox}$;*Suv4-20h2*$^{-/-}$;*ROSA26* mouse colonies for experiments. Genotyping utilized tissues from ear punch. Ear punch samples were lysed in 90 uL of fresh-made 50 mM NaOH shaking at 95.0°C for 10 min. After 10 min, samples were cooled on ice and NaOH was neutralized immediately with 10 uL 1M Tris HCL, briefly vortexing. Samples can be used immediately for genotyping or stored at −20°C. PCR cocktail includes: 25 uL Apex Taq RED Master Mix (Genesee Scientific, Cat #: 42–137), 1 uL per primer, 1 uL template DNA, bring to 50 uL with nuclease free water. Thermocyler program was as follows: 1 cycle: 95.0°C @ 3 min; 25–35 cycles: 95.0°C @ 20 sec, 58°C @ 40 sec, 72.0°C @ 1 min; 1 cycle: 72°C @ 7 min, hold at 4°C. Visualize amplicons using 1 – 1.5% agarose gel in 1X TAE with 0.5 ug/mL final concentration of EtBr in gel (100 V for 45 – 90 min for separation of bands). All mouse strains were congenic prior to experiments. Mice (males and females) between 12 and 24 weeks old were used. All animal experiments were approved by the Institutional Animal Care and Use Committee of the University of Texas at San Antonio (UTSA).

Cre protein induction and purification

For Cre protein induction and purification, His-Cre-CTP was transformed into BL21(ED3)pLysS (Invitrogen) for protein expression. The overnight bacterial culture was inoculated at dilution of 1:80 in LB with 100 mg/mL ampicillin for 2 hours at 37°C and proteins were induced with 0.5 mM IPTG for 2 hr at room temperature. Total protein was extracted with lysis buffer (50 mM NaH_2PO_4, pH 8, 0.5 M NaCl, 10 mM imidazole, 0.2% Triton X-100, 6 mM 2-mercaptoethanol) and purified with Ni-NTA superflow cartridge (Qiagen). After wash with buffer containing 50 mM NaH_2PO_4, pH 8.0, 0.3 M NaCl, 20 mM imidazole, Cre protein was eluted with elution buffer (250 mM imidazole in PBS). The eluted protein fractions went through buffer exchange with PBS using 10 K Amicon centrifugal filter (Millipore) and then stored in 20% glycerol/PBS at −80°C. Protein concentration was determined by Bradford Assay (BioRad).

Stereotaxic injection of Cre-CTP protein and vehicle solutions

Experimental design: For external controls, *ROSA26* "reporter" mice were utilized which only have the lacZ or YFP reporter (R26R-lacZ or R26R-EYFP), but do not have conditional alleles for *Ezh2*$^{flox/flox}$ or *Suv4-20h1*$^{flox/flox}$;*Suv4-20h2*$^{-/-}$. These mice were injected with Cre and the phenotypic effect were compared to animals harboring *Ezh2*$^{flox/flox}$:*ROSA26* or *Suv4-*

20h1$^{flox/flox}$;*Suv4-20h2*$^{-/-}$;*ROSA26* that have also been injected with Cre. For internal controls, one hemisphere of the brain was injected with vehicle (20% glycerol in PBS) and the contralateral hemisphere was injected with Cre protein. Phenotypes were then compared among conditional knock-out (cKO) of *Ezh2*, cKO of *Suv4-20h*, and both internal and external controls.

Mice were anesthetized with 2% isoflurane at a flow rate of 0.5 L/min. Upon reaching a deep plane of anesthesia, mice were centered on a model 1900 stereotaxic frame (KOPF Model 1900 stereotax). Prior to Cre injections, 10 mg/kg Lidocaine and 2 mg/kg Marcaine solutions were administered by subcutaneous injection at incision site, prior to a 1 cm incision being cut along the dorsomedial scalp to expose the frontal and parietal bones between Bregma and Lambda landmarks. Subsequently, 5 mg/Kg Baytril was administered by IP injection. Bore holes of 0.53 mm diameter were drilled into the mouse skull at the appropriate A/P and M/L coordinates using a #75 drill bit on a model 1911 stereotaxic drill (KOPF). Using a custom-made Hamilton Neuro syringe with a 12° beveled tip (custom-made Hamilton 0.5 uL, Neuro model 7000.5 KH syringe including a 32 gauge needle with Point Style 4, hamiltoncompany.com, Cat #: 65457-02), Cre was injected into the SVZ including 4 injection sites per hemisphere per mouse at the following coordinates: anteroposterior (+0.97; +0.49; +0.25; −0.11), mediolateral (±0.95; ±1.32; ±1.35; ± 1.5), and dorsoventral (−2.6; −2.2 −2.15; −2.0). The coordinates for SGZ/DG stereotaxic injection are anteroposterior (−1.50; −2; −2.53; −2.91), mediolateral (±1.50; ±1.62; ±1.68; ±1.8), and dorsoventral (−1.95; −2.1; −2.1; −2.22). All coordinates are measured from the Bregma landmark on exterior of the balanced skull. After needle placement at proper coordinates, 350 nL Cre or vehicle was infused at each injection site from the Hamilton syringe at a rate of 60–100 nL/min using a UltraMicroPump driven by a SYS-Micro4 controller (World Precision Instruments). Following a 5 min post-injection recovery period, the mice were returned to normal habitat containing a DietGel gel cup with Caprophen tablets (10 mg/kg PO). A 4 day post-surgical period ensured complete degradation of EZH2 or Suv4-20h protein that had been translated prior to Cre mediated knockout.

Gene expression analysis

For qRT-PCR validation, total RNA was extracted from the SGZ/DG using TRIzol (Invitrogen) reagent followed by aqueous/organic phase separation, isopropyl alcohol RNA precipitation, dissolving RNA with 25–50 uL nuclease free water and subsequently cDNA synthesis by iScript reverse transcriptase supermix (Bio-Rad, #170-8841) according to the manufacturer's instructions. Briefly, 5 uL input RNA (1 pg – 1 ug) was combined with 4 uL iScript supermix and brought to 20 uL total volume with nuclease free water. RT reaction protocol is as follows: priming: 5 min @ 25°C; RT: 20 min @ 46°C; inactivation: 1 min @ 95°C. The transcript expression level was measured by Real-Time PCR with SYBR Select Master Mix (Life Technologies, #4472908) and detection on ABI7900HT system (Applied Biosystems). S16 RNA was used as internal control for normalization (ΔCt). The differential expression was measured by subtraction of ΔCt between wildtype and *Ezh2* knockout animals to obtain ΔΔCt (log2). Primers were designed using ABI Primer Express Software version 3.0, PrimerBank (https://pga.mgh.harvard.edu/primerbank/), and Primer3Plus (http://www.bioinformatics.nl/cgi-bin/primer3plus/primer3plus.cgi). At least one primer pair per gene spanned 2 or more exons.

Immunohistochemistry

Mice were anesthetized with 450 mg/Kg Avertin, transcardially perfused with 1x PBS, and fixed with 4% paraformaldehyde. Following fixation, mouse brains were cryopreserved with 30% sucrose/PBS overnight and frozen in OCT compound. Frozen brains were sectioned at 12 μm, blocked with 10% goat serum for 30 minutes, and incubated 4°C overnight with combinations of antibodies specific for: H3K27me3 (Active Motif, Cat#39155;Lot#31814017, 1:1000), β-galactosidase (Promega, Cat#z378B;Lot#0000040733, 1:750), GFP (Invitrogen, Cat#A11122, 1:500; Aves Labs, Cat#GFP-1020;Lot#1229FP08, 1:500), and cell type specific markers: GFAP (Millipore, Clone GA5, Cat#mab3402, Lot#2580632, 1:750), Nestin (AbCam, Cat#ab27952, 1:300; AbCam, Cat#ab134017, 1:250), DCX (Santa Cruz, Cat#sc-8066; Lot#10314, 1:200), βIII-Tubulin (Millipore, clone TU-20, Cat#MAB1637, Lot#JC1686015, 1:200), and NeuN (Millipore, clone A60, Cat#MAB377, Lot#NG1876252, 1:200). On the subsequent day, sections were washed with 0.5% TritonX-100/1X PBS. Following wash, antibody combinations needing only secondary antibodies (i.e. H3K27me3, GFAP, GFP, chicken anti-Nestin, and/or DCX) were incubated with AlexaFlour-488 or −594 conjugated secondary antibodies (anti-mouse: Life Technologies, Cat#A21200; Life Technologies, Cat#A21201; anti-rabbit: Invitrogen, Cat#A21441; Life Technologies, A21207, anti-chicken Life Technologies, Cat#A11039, anti-goat: Life Technologies Cat#A11055; Life Technologies, Cat#A11058). Sections probed with all other antibodies (rabbit anti-Nestin; mouse anti-βIII-Tubulin, NeuN, β-gal) were incubated with Biotinylated-rabbit or –mouse secondary antibody for 1 hour at room temperature (Vector Laboratories, Cat#BA-1000, 1:1000; Vector Laboratories, Cat#BA-2000, 1:1000), followed by Avidin-conjugated AlexaFlour-488 or Avidin-conjugated AlexaFlour-594 tertiary antibody for 1 hour (Life technology, Cat#A21370, 1:2000; Life technology, Cat#S32356, 1:2000). Analysis of thymidine analog incorporation involved administration of EdU (5-ethynyl-2'-deoxyuridine) into mice by intraperitoneal (IP) injection 2 hours prior to perfusion. EdU was detected by Click-iT EdU 488 or 647 imaging kits (Invitrogen, C10337; Invitrogen, C10640), following manufacturer's instructions. All sections were mounted with Vectashield mounting medium with DAPI (Vector Laboratories, Cat# H-1200). Images were acquired on a either a Zeiss 510 or 710 confocal microscope with 20X, 40X, and 63X objectives and were processed using the associated analysis software, Zen. Scale bars were added by ImageJ (https://imagej.nih.gov/ij/).

Flow cytometry

Mice were anesthetized with 450 mg/Kg Avertin prior to decapitation. Freshly isolated SGZ/DG cells were fixed with 4%

paraformaldehyde, permeabilized, incubated 4°C overnight with primary antibodies (anti-GFAP, Nestin, PSA-NCAM, Doublecortin, NeuN, H3K27me3, S100-β, and ALDH1L1), and subsequently labeled with BV421, PE, PE-Cy7 (BD Biosciences) and Alexa fluor 488, −594, −647 (Life Technologies) conjugated secondary antibodies. Primary antibody sources: Doublecortin (Cell Signaling #4604; Millipore clone2G5 MABN707, 1:500), Polysialic Acid Neural Cell Adhesion Molecule PSA-NCAM, clone 2-2b (Millipore #MAB5324, Lot# 1966892, 1:500), Glial Fibrillary Acidic Protein GFAP, clone GA5 (Millipore #MAB3402, Lot#1993774, 1:500; Abcam clone 2A5 #ab4648, 1:500), Nestin (Abcam #AB27952; 1:500), NeuN (Millipore MAB377, 1:500). H3K27me3 (Active Motif, 1:1000), S100-β (AbCam, Cat#ab41548 1:500), β-galactosidase (Promega, Cat#z378B, 1:750). Secondary antibody sources: BD Biosciences. Analysis of thymidine analog incorporation involved administration of BrdU (5-bromo-2′-deoxyuridine) and EdU (5-ethynyl-2'-deoxyuridine) into mice by intraperitoneal (IP) injection 5 days post-injection and 2 hours prior to dissection, respectively. For BrdU detection, following paraformaldehyde fixation, cells were treated with 1.5N HCl, incubated with anti-BrdU primary (Life Technologies, #033900, 1:100) and labeled with Alexa fluor-647 (anti-mouse: Life Technologies, Cat#A21463, 1:300) conjugated secondary. EdU was detected by Click-iT EdU 647 imaging kit (Invitrogen, C10340), following manufacturer's instructions. For analysis, controls included single color controls stained with each antibody separately, unstained cells for gate placement, and compensation beads for spectral compensation. Briefly, a drop of OneComp eBeads (eBioscience 01-1111-42) was incubated with 1 ul of fluorochrome-conjugated anti-mouse antibody for 15 – 30 min on ice and protected for light. Beads were washed with 1 mL of cell staining buffer and resuspended in 300 ul of same buffer prior running the samples on an LSR-II cytometer. Flow cytometry data was acquired on a LSR-II (BD Biosciences) configured with an argon 488 laser with a 505 LP dichroic and 525/50 filter to detect Alexa fluor 488 and a green 510 laser with a 735 LP dichroic and a 575/26 filter to detect PE. Compensation and data analysis was performed using FlowJo software (Tree Star, Inc, Ashland, OR).

Imaging flow cytometry

Mice were anesthetized with 450 mg/Kg Avertin prior to decapitation. Following euthanasia, the dentate gyrus was dissected under microscope, dissociated into single cells by Accutase, and passed through a 40 um cell strainer. Cells were subsequently fixed by 4% paraformaldehyde, blocked with 10% goat serum, incubated 4°C overnight with antibody against GFP (Invitrogen, Cat#A11122, 1:250; Aves Labs, Cat#GFP-1020; Lot#1229FP08, 1:500), H4K20me3 (AbCam, Cat#ab9053), MCM2 (Santa Cruz, Cat#sc-9839), p-H3(S10) (Millipore, Cat#06-570), p-s780-Rb (Cell Signaling, Cat#9307S), NeuN (Millipore, clone A60, Cat#MAB377, Lot#NG1876252, 1:200), subsequently washed with Perm/Wash buffer (BD Biosciences, Cat#554723) and incubated with anti-mouse AlexaFluor-488, AlexaFluor-647 (Life Technologies, Cat#A21200), and anti-rabbit PE (BD Biosciences). Analysis of thymidine analog incorporation involved administration of EdU (5-ethynyl-2'-deoxyuridine) into mice by intraperitoneal (IP) injection 12 hours prior to dissection. EdU was detected by Click-iT EdU 488 or 647 imaging kits (Invitrogen, C10337; Invitrogen, C10340), following manufacturer's instructions. Processed cells were imaged by Amnis ImageStreamX MKII imaging flow cytometer and quantified with associated IDEAs software.

Tissue clearing and light sheet microscopy

The new iDISCO+ protocol (May 2016, https://idisco.info/idisco-protocol/update-history/) was followed for all steps and reagents used during tissue fixing, immunohistochemistry and clearing. Briefly, mice were perfusion fixed with PBS and 4% paraformaldehyde (PFA) followed by overnight incubation in 4% PFA in 4°C. Brains were cut into 2 mm sagittal blocks in a brain matrix (Braintree Scientific, BS-A 5000S) prior to clearing. Following overnight fixing with 4% PFA, brains were pretreated with methanol (Fisher A412-4) and bleached with 30% hydrogen peroxide (Sigma 216763-100ML) on an orbital rocker. For immunohistochemistry, doublecortin was detected using goat anti-doublecortin primary (Santa Cruz, sc-8066, 1:200) and Alexa Fluor 594-conjugated secondary antibodies (Life Technologies, A11058, 1:200). NeuN detection utilized mouse anti-NeuN (Millipore, MAB377, 1:200), biotinylated secondary (Vector Laboratories, BA-2000, 1:200) and Alexa Fluor 488-conjugated avidin (Life Technologies, A21370, 1:200). For all steps prior to tissue clearing, incubation times (listed as "n" in iDISCO+ protocol)/ Solution volume followed table in iDISCO+ protocol and were as follows: 3 day/ 4 mL for 2 mm sagittal mouse sections. Tissue clearing involved methanol dehydration series and overnight 66%:33% methanol: Dichloromethane (DCM) incubation, and clearing with 100% DCM (Sigma 270997-1L) and Dibenzyl Ether (DBE) (Sigma 108014-1KG). Cleared tissues were imaged on an Ultramicroscope, LaVision BioTec light sheet microscope (LaVision, Bielefeld, Germany) and were processed with Imaris software (Imaris x64 8.1.2).

Image quantification

All steps of light sheet imaging quantification were performed in ImageJ following manufacturer's example in "Area Measurements and Particle Counting" (https://imagej.nih.gov/ij/docs/pdfs/examples.pdf). Mean fluorescence intensity (MFI) was determined by splitting RGB Color images into 8-bit greyscale images using the Split Channels tool before auto-adjusting with the Threshold setting. After thresholds were set, the Analyze Particles tool detected the average pixel intensity per area within the threshold range. The sizes used for particle analysis were 100-Infinity.

Statistics

For flow cytometry, two-sample t-tests were performed in R (https://cran.r-project.org/). For differential expression, a moderated t-test was performed using empirical Bayes moderation of the standard errors using the ebayes function of limma package in R/Bioconductor (https://bioconductor.org/packages/release/bioc/html/limma.html).

Acknowledgments

We thank Drs. Alexander Tarakhovsky and Gunnar Schotta for generously providing conditional *Ezh2* and *Suv4-20h* mouse lines, respectively. Authors are grateful to Dr. Fred Gage for his insightful comments and technical support. We also thank Drs. Arturo Alvarez-Buylla, Douglas Grow, ChiungYu Hung, and Sebastian Jessberger for technical advice. Stereotaxic injections, confocal imaging, and flow cytometry/imaging flow were done in the Neuroscience Institute Opto-excitability Core Facility, the Imaging Core, and the Immune Defense Core at UTSA, respectively. Light Sheet Fluorescent Microscopy was conducted in The Miami Project to Cure Paralysis Image Analysis Core. CTR and SAH were supported by NIH/NIGMS SC3GM112543. SMC and AEC were supported by NIH/NIGMS SC1GM095426 and NIH/NINDS NS078501. GZ and VPL were supported by The Walter G. Ross Foundation and NIH/NICHD HD057632. This project was supported by NIH/NIGMS SC3GM112543 and TRAC award to CAL.

Author contributions

CTR performed stereotaxic injection and preparation of figures and manuscript. GZ performed light sheet imaging and processing by Imaris. CTR, GZ, and SAH performed experiments including modified iDISCO, IHC, and confocal imaging. CTR, SMC, and AEC performed flow cytometry and analysis. CAL, CTR, and SAH performed Cre protein purification. MSB and VPL contributed to provision of materials, data interpretation, and manuscript preparation. CAL contributed to project management, provision of materials, conception and design of experiments. CAL wrote manuscript with comments from all authors.

Disclosure of potential conflict of interest

The authors declare no competing financial interests.

Funding

HHS | NIH | National Institute of General Medical Sciences (NIGMS) [grant number NIH/NIGMS SC3GM112543]

References

[1] Alvarez-Buylla A, Lim DA. For the long run: maintaining germinal niches in the adult brain. Neuron. 2004;41:683-686. 10.1016/S0896-6273(04)00111-4. PMID:15003168

[2] Bond AM, Ming GL, Song H. Adult mammalian neural stem cells and neurogenesis: five decades later. Cell Stem Cell. 2015;17:385-395. 10.1016/j.stem.2015.09.003. PMID:26431181

[3] Kempermann G, Song H, Gage FH. Neurogenesis in the adult hippocampus. Cold Spring Harbor Perspec Biol. 2015;7:a018812. 10.1101/cshperspect.a018812. PMID:26330519

[4] Hirabayashi Y, Suzki N, Tsuboi M, et al. Polycomb limits the neurogenic competence of neural precursor cells to promote astrogenic fate transition. Neuron. 2009;63:600-613. 10.1016/j.neuron.2009.08.021. PMID:19755104

[5] Pereira JD, Sansom SN, Smith J, et al. Ezh2, the histone methyltransferase of PRC2, regulates the balance between self-renewal and differentiation in the cerebral cortex. Proc Nat Acad Sci United States Am. 2010;107:15957-15962. 10.1073/pnas.1002530107. PMID:20798045

[6] Sher F, Boddeke E, Olah M, et al. Dynamic changes in Ezh2 gene occupancy underlie its involvement in neural stem cell self-renewal and differentiation towards oligodendrocytes. PloS One. 2012;7:e40399. 10.1371/journal.pone.0040399. PMID:22808153

[7] Xie W, Schultz MD, Lister R, et al. Epigenomic analysis of multilineage differentiation of human embryonic stem cells. Cell. 2013;153:1134-48. 10.1016/j.cell.2013.04.022. PMID:23664764

[8] Foret MR, Sandstrom RS, Rhodes CT, et al. Molecular targets of chromatin repressive mark H3K9me3 in primate progenitor cells within adult neurogenic niches. Front Genet. 2014;5:252. 10.3389/fgene.2014.00252. PMID:25126093

[9] Yao B, Jin P. Unlocking epigenetic codes in neurogenesis. Genes Dev. 2014;28:1253-1271. 10.1101/gad.241547.114.

[10] Rhodes CT, Sandstrom RS, Huang SA, et al. Cross-species analyses unravel the Complexity of H3K27me3 and H4K20me3 in the context of neural stem progenitor cells. Neuroepigenetics. 2016;6:10-25. 10.1016/j.nepig.2016.04.001. PMID:27429906

[11] Schotta G, Sengupta R, Kubicek S, et al. A chromatin-wide transition to H4K20 monomethylation impairs genome integrity and programmed DNA rearrangements in the mouse. Genes Dev. 2008;22:2048-2061. 10.1101/gad.476008.

[12] Su IH, Basavaraj A, Krutchinsky AN, et al. Ezh2 controls B cell development through histone H3 methylation and Igh rearrangement. NatImmunol. 2003;4:124-31. 10.1038/ni876. PMID:12496962

[13] Hwang WW, Salinas RD, Siu JJ, et al. Distinct and separable roles for EZH2 in neurogenic astroglia. eLife. 2014;3:e02439. 10.7554/eLife.02439. PMID:24867641

[14] Zhang J, Ji F, Liu Y, et al. Ezh2 regulates adult hippocampal neurogenesis and memory. J Neurosci Off J Soc Neurosci. 2014;34:5184-5199. 10.1523/JNEUROSCI.4129-13.2014. PMID:24719098

[15] Eberling JL, Wu C, Tong-Turnbeaugh R, et al. Estrogen- and tamoxifen-associated effects on brain structure and function. NeuroImage. 2004;21:364-371. 10.1016/j.neuroimage.2003.08.037. PMID:14741674

[16] Chen HY, Yang YM, Han R, et al. MEK1/2 inhibition suppresses tamoxifen toxicity on CNS glial progenitor cells. J Neurosci Off J Soc Neurosci. 2013;33:15069-15074. 10.1523/JNEUROSCI.2729-13.2013. PMID:24048837

[17] Chen X, Li J, Chen J, et al. Decision-making impairments in breast cancer patients treated with tamoxifen. Horm Behav. 2014;66:449-456. 10.1016/j.yhbeh.2014.07.005. PMID:25036869

[18] Schilder CM, Seynaeve C, Beex LV, et al. Effects of tamoxifen and exemestane on cognitive functioning of postmenopausal patients with breast cancer: results from the neuropsychological side study of the tamoxifen and exemestane adjuvant multinational trial. J Clin Oncol Off J Am Soc Clin Oncol. 2010;28:1294-1300. 10.1200/JCO.2008.21.3553. PMID:20142601

[19] Renier N, Wu Z, Simon DJ, et al. iDISCO: a simple, rapid method to immunolabel large tissue samples for volume imaging. Cell. 2014;159:896-910. 10.1016/j.cell.2014.10.010.

[20] Will E, Klump H, Heffner N, et al. Unmodified Cre recombinase crosses the membrane. Nucleic Acids Res. 2002;30:e59. 10.1093/nar/gnf059. PMID:12060697

[21] Lin Q, Jo D, Gebre-Amlak KD, et al. Enhanced cell-permeant Cre protein for site-specific recombination in cultured cells. BMC Biotechnol. 2004;4:25. 10.1186/1472-6750-4-25. PMID:15500682

[22] Chien WM, Liu Y, Chin MT. Genomic DNA recombination with cell-penetrating Peptide-tagged Cre Protein in mouse skeletal and cardiac muscle. Genesis. 2014;52(7):695-701. 10.1002/dvg.22782. PMID:24753043

[23] Cao G, Pei W, Ge H, et al. In vivo delivery of a Bcl-xL fusion protein containing the TAT protein transduction domain protects against ischemic brain injury and neuronal apoptosis. J Neurosci Off J Soc Neurosci. 2002;22:5423-31. PMID:12097494

[24] Xi J, Liu Y, Liu H, et al. Specification of midbrain dopamine neurons from primate pluripotent stem cells. Stem Cells. 2012;30:1655-63. 10.1002/stem.1152. PMID:22696177